Downloaded from orbit.dtu.dk on: Apr 24, 2025

DTU Library

Effect of Molecular Weight on the Feature Size in Organic Ice Resists

Elsukova, Anna; Han, Anpan; Zhao, Ding; Beleggia, Marco

Published in:
Nano Letters

Link to article, DOI:
10.1021/acs.nanolett.8b03130

Publication date:
2018

Document Version
Peer reviewed version

Link back to DTU Orbit

Citation (APA):
Elsukova, A., Han, A., Zhao, D., & Beleggia, M. (2018). Effect of Molecular Weight on the Feature Size in Organic Ice Resists. *Nano Letters*, *18*(12), 7576-7582. https://doi.org/10.1021/acs.nanolett.8b03130

General rights
Copyright and moral rights for the publications made accessible in the public portal are retained by the authors and/or other copyright owners and it is a condition of accessing publications that users recognise and abide by the legal requirements associated with these rights.

- Users may download and print one copy of any publication from the public portal for the purpose of private study or research.
- You may not further distribute the material or use it for any profit-making activity or commercial gain
- You may freely distribute the URL identifying the publication in the public portal

If you believe that this document breaches copyright please contact us providing details, and we will remove access to the work immediately and investigate your claim.

Effect of molecular weight on the feature size in organic ice resists

Anna Elsukova[1], Anpan Han[2], Ding Zhao[1], and Marco Beleggia[1]*

[1]DTU Danchip/Cen, Technical University of Denmark, 2800 Kongens Lyngby, Denmark

[2]DTU Mechanical Engineering, Technical University of Denmark, 2800 Kongens Lyngby, Denmark

* marco.beleggia@cen.dtu.dk

Table of Contents Graphic

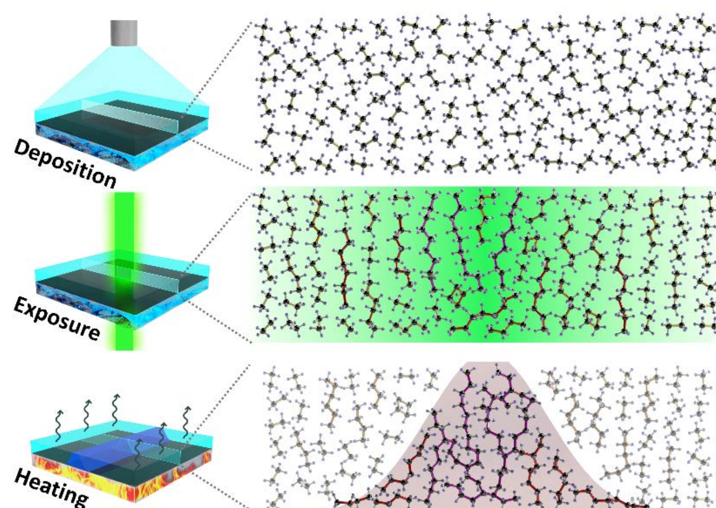

Abstract

The feature size of patterns obtained by electron beam lithography (EBL) depends critically on resist properties, beam parameters, development process, and instrument limitations. Frozen layers of simple organic molecules such as n-alkanes behave as negative tone resists for EBL. With the unique advantage of an in-situ thermal treatment replacing chemical development, the entire lithographic process can be performed within a single instrument, thus removing the influence of chemical developers on the feature

size. By using an environmental transmission electron microscope, we can also minimize the influence of instrumental limitations and explore the fundamental link between resist characteristics and feature size. Our results reveal that the onset dose of organic ice resists correlates with the inverse molecular weight, and that in the thermal development the role of change in solubility of polymers is mirrored in a shift in the solid/vapour critical temperature of organic ices. With a 0.4 pA beam current we obtained 4.5 nm, 5.5 nm, 8.5 nm, lines with frozen octane, undecane, and tetradecane, respectively, consistent with the predictions of a model we developed that links beam profile and feature size. The knowledge acquired on the response of small organic molecules to electron irradiation, combined with the flexibility and operational advantages of using them as qualified EBL resists, provide us with new opportunities for the design and production of nanodevices, and broadens the reach of EBL especially towards biological applications.

Keywords

E-beam lithography, organic ice resist, condensed organic molecules, crosslinking, transmission electron microscopy, exposure mechanism

During the last 50 years electron beam lithography (EBL) has advanced significantly, and can now deliver structures that are just a few nanometers in size. EBL is used in many research areas such as advanced electronics,[1] quantum computing[2], nanophotonics[3], 2D material devices[4], optomechanical[5] and nanofluidics systems[6]. EBL is also expanding into the patterning of biomolecules[7,8], with potential applications ranging from tissue engineering, to drug delivery, to fabrication of biosensors and bio-interfaces for diagnostics and cell stimulation[9,10]. An emerging trend in many application fields is three-dimensional (3D) device fabrication[11]. To satisfy the broad range of practical demands, new resist materials[12] and approaches to

electron-beam (e-beam) based nanopatterning are being considered[13,14]. In this perspective, we have recently introduced the concept of Organic Ice Resists (OIR)[15]. Instead of conventional spin-coating and chemical development, we first freeze simple organic molecules at cryogenic temperature (Figure 1a,b), and then expose them to a focused electron beam (Figure 1c), leading to crosslinking of the molecules (Figure 1d). After thermal development by heating the sample, light molecules will leave the substrate while heavily crosslinked molecules within the exposure area are solidified (Figure 1e,f). Therefore, these organic materials can act as negative-tone resists in EBL. Repeated condensation–exposure cycles yielding 3D layered structures can be efficiently fabricated *in a single instrument*[16,17]. The use of biocompatible organic materials and the chemical-free development process could potentially make OIR-based lithography (OIRL) the most convenient method for nanofabrication of bio-devices. Finally, OIRL handles easily substrates with complex morphologies (for example, a thin microporous Si_3N_4 membrane[15]). Since the resist material condenses from vapor, it can be uniformly deposited on porous, grooved and curved surfaces *in a single step*. This is particularly important for nanofluidic applications, and is currently beyond the reach of conventional EBL or nanoimprint patterning protocols[18].

In this work, we take the first steps towards a deeper understanding of the principles behind e-beam exposure of organic ices, and of the role played by the thermal development. Acquiring knowledge on the radiation chemistry processes driving the OIR exposure mechanism, and on how it relates to the characteristics of the patterns, is crucial for identifying the optimal organic material, lithographic protocol and control over the structures' functionality in view of specific applications. The fundamental question we address here is what controls the feature size achievable in OIRL, and how it relates to the initial molecular weight of the chosen organic compound. For this purpose, we have chosen to pattern the smallest and the simplest organic molecules with suitable freezing points: linear hydrocarbons octane C_8H_{18}, undecane $C_{11}H_{24}$, and tetradecane $C_{14}H_{30}$ (Figure 1g). These molecules have a simple linear structure with only C-C and C-H bonds. Therefore, we expect their molecular weight to be the key parameter determining the patterned feature size.

To minimize the influence of instrumental limitations on the feature size, for example a broad beam spot and optics instabilities, we used an environmental transmission electron microscope (ETEM)[19] equipped with a gas cell and a cryo-holder to condense OIR on a 5-nm thick Si_3N_4 membrane, and operated at 80 keV. Images of the resulting OIR patterns were obtained in-situ, immediately after the substrate was heated. The microscope optics allowed us to change the e-beam current continuously and independently from the beam spot size. The spot size in a TEM operated in scanning mode is controlled by the C2 (second condenser) aperture and by the excitation of the objective lens, situated below. The beam current is set by adjusting the strength of the lenses above the C2 aperture, which disperses and condenses the illumination on it, thereby changing the number of electrons passing through without affecting the spot size. Therefore, we could set a small beam spot (~1 nm) and study the patterned linewidth as function of dose. The beam current was measured using a calibrated CCD camera by counting the total number of electrons detected over a given exposure time. This is equivalent to measuring the current by a Faraday cup. The experimental setup and procedure are described in detail in the Supporting Information. Figure 1h shows a simplified diagram of the phase transitions occurring during the OIRL process. First, an organic vapor is condensed into an amorphous ice layer at temperature T_{LN2}. Then, electron beam irradiation initiates the breakdown of chemical bonds of the original molecules, leading to their subsequent crosslinking. After crosslinking, the irradiated region has a larger average molecular weight and thus higher sublimation temperature T_{sub}. After heating to temperature T_h, all molecules with $T_{sub}>T_h$ remain on the substrate. We do not observe any liquid phase present after heating. However, it is possible that they could form and evolve during heating (not shown in Figure 1h). The final products of the OIRL process are hydrogen containing carbonaceous structures, which are non-volatile, chemically inert and very stable at ambient conditions[15].

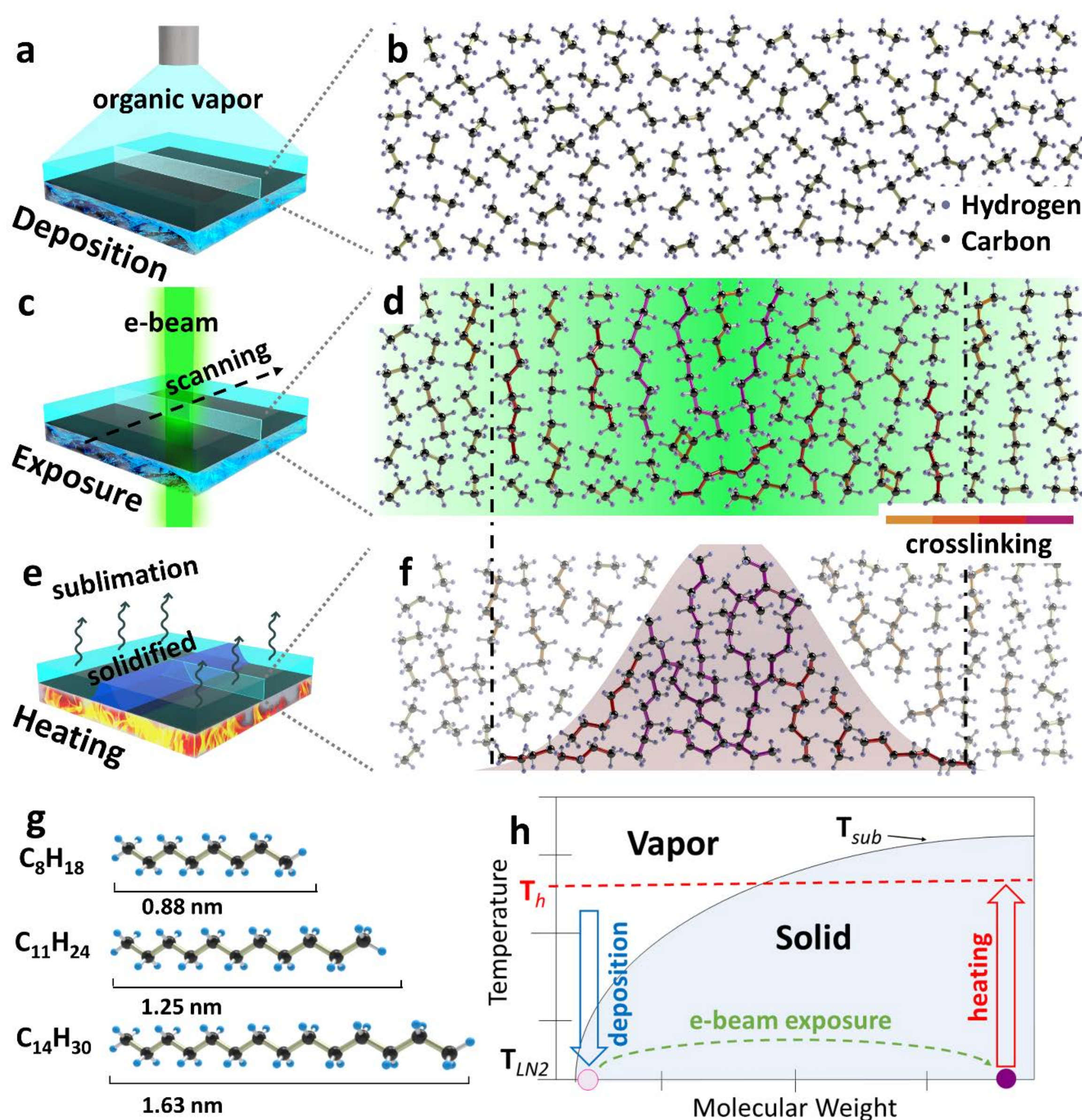

Figure 1. Organic ice resists lithography and interactions between electron beam and ice resists. (a) A layer of deposited amorphous organic ice (light blue) on a cold substrate surface and (b) an illustration of its cross sectional view. (c) Exposing the ice layer to a focused electron beam (green) with a Gaussian profile leads to (d) crosslinking of the molecules. The electron beam current density decreases gradually from the center (dark green) out to the periphery (light green), and the degree of crosslinking depends on the received dose. The dash-dot lines represent the borders within which organic ice receives enough dose to form a non-volatile product at T_h. (e) The solidified line pattern (dark blue) that remains within the scanned area after heating the sample to temperature T_h (40 ^oC). (f) The approximate cross-sectional profile of the line pattern (shaded area). The pattern thickness is proportional to the number of molecules crosslinked enough to become non-volatile at T_h. (g) Molecular dimensions of the linear hydrocarbons octane C_8H_{18}, undecane $C_{11}H_{24}$, and tetradecane $C_{14}H_{30}$. (h) Simplified phase diagram underpinning the OIRL process.

After testing and adjusting the deposition parameters, we deposited a thin (12–15 nm) layer of ice and found the patterning conditions that delivered the smallest linewidths. Figure 2 shows parallel lines patterned on octane (a-c), undecane (d-f) and tetradecane (g-i) using beam currents I_{0L} of 0.4 pA (a, d, g), 0.66 pA (b, e, h) and 1.6 pA (c, f, g), and dwell time per dot τ_L=10 ms. The line dose is defined as $D=I_{0L}\tau_L/\Delta x_L$, where $\Delta x_L=L/N$, L=360 nm is the length of the line, N=100 is the number of dots. We carefully estimated the linewidths from bright-field TEM images by fitting the out-of-focus intensity profile with an analytical model for a Gaussian weak phase object. Details on linewidth estimation from TEM images are discussed in the Supporting Information. In our previous work[15], we characterized the resulting patterns with Energy Dispersive X-ray (EDX) and Electron Energy-Loss (EELS) spectroscopies. EDX showed only presence of carbon, and the EELS carbon K-edge had the typical shape of hydrogenated carbon in an amorphous environment. Hydrogenated carbon produces a weak contrast in TEM and is prone to beam damage, which leads to carbon sputtering and thinning of structures. To minimize damage and increase the contrast, we imaged the structure under-focus at low-dose.

The experimental data show two trends: 1) the linewidth decreases with the beam current (line dose) (Figure 2 j), and 2) for a fixed beam current (line dose), the linewidth decreases with the decreasing initial molecular weight of the precursor (Figure 2k). The smallest linewidth of 4.5 nm was achieved on octane using a beam current of 0.4 pA (Figure 2a).

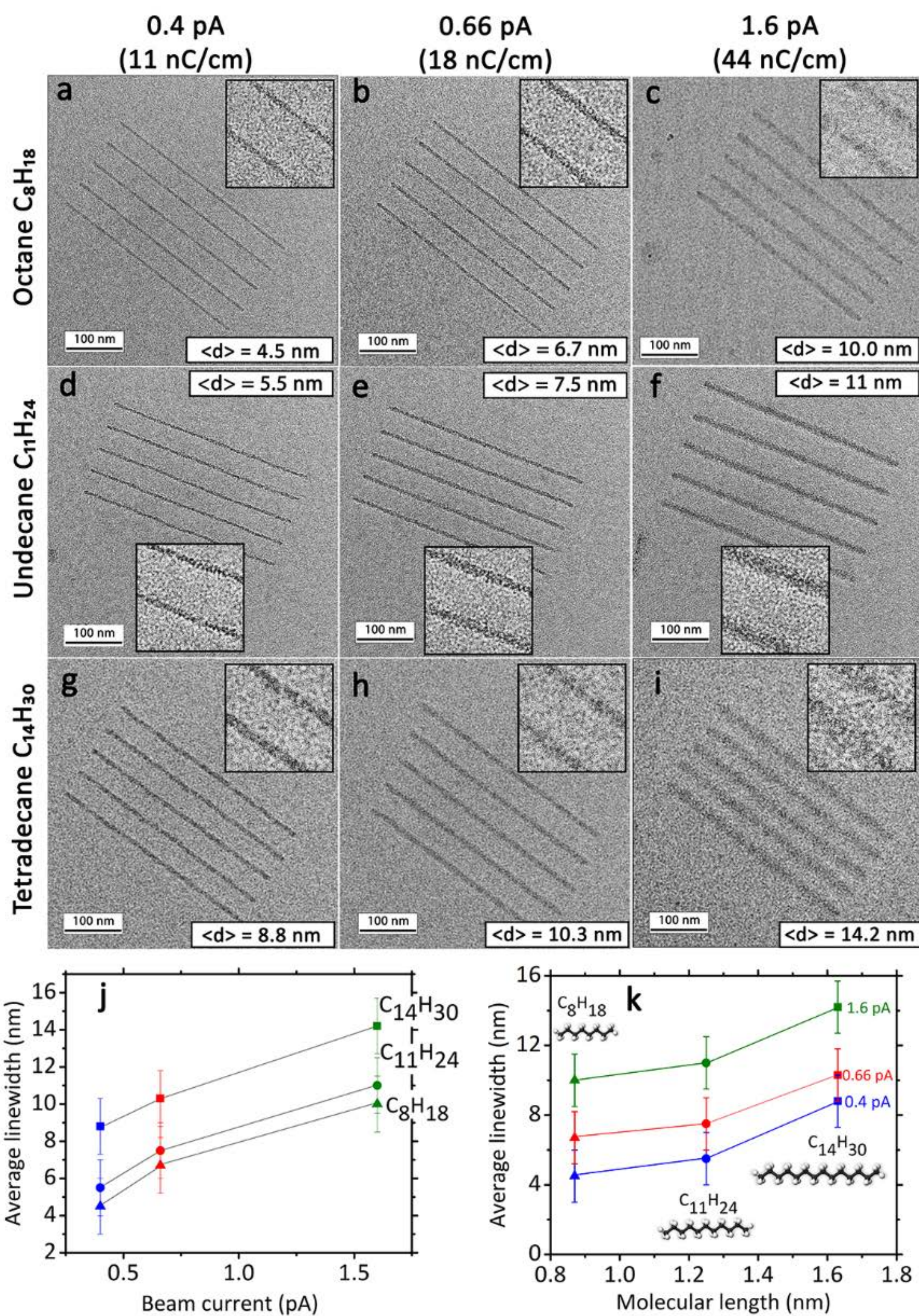

Figure 2. Parallel lines patterned on octane (a)-(c), undecane (d)-(f) and tetradecane (g)-(i) OIRs using beam currents 0.4 pA (a, d, g), 0.66 pA (b, e, h) and 1.6 pA (c, f, g). Patterning parameters: line length L=360 nm, dwell time per dot τ_L=10 ms, number of dots N=100. Line dose is defined as $D=I_{0L}\tau_L/\Delta x_L$, where I_{0L} is the beam current, $\Delta x_L=L/N$. Bottom row: Average linewidths of the patterned structures plotted as a function of (j) beam current and (k) OIR precursor molecular length.

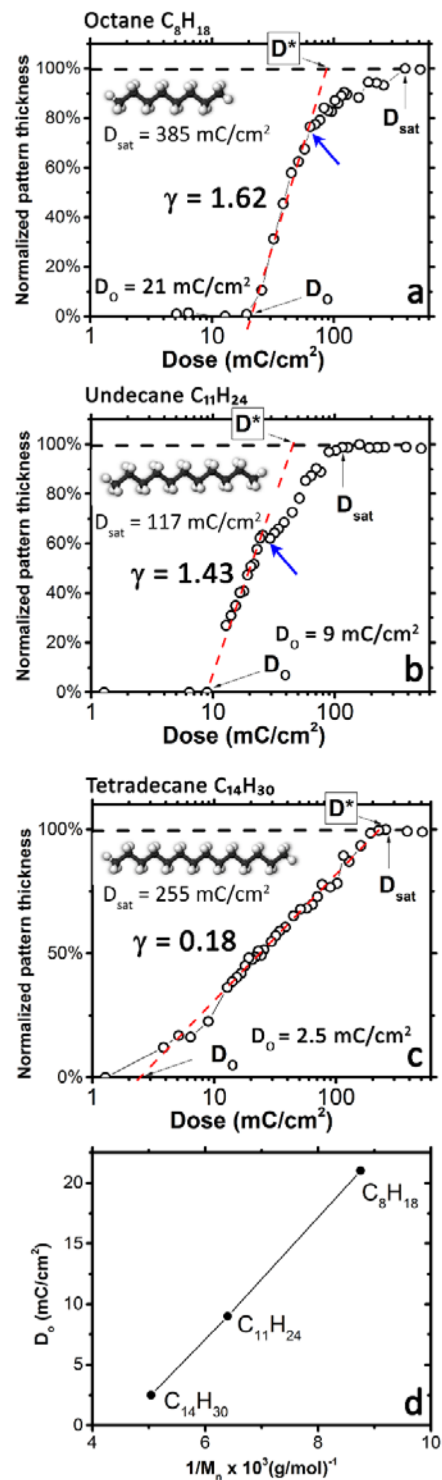

Figure 3. Contrast curves for (a) octane, (b) undecane and (c) tetradecane OIRs. (d) Onset dose (D_O) dependence on OIR molecular weight. The pattern thickness is normalized to the thickness of a highly exposed area. Contrast $\gamma=1/\log_{10}(D^*/D_O)$, where D_O and D^* are determined by extrapolating the linear portion of the contrast curve to 0 and 100%, respectively. D_{sat} represents a saturation dose. Blue arrows in (a, b) highlight a visible change of slope in the contrast curve.

To gain insight into the exposure mechanism of organic ices, we acquired a set of contrast curves (Figure 3a-c) for the three compounds examined. We patterned 500x500 nm^2 squares with a beam current of 3 pA. Patterning was carried out by obtaining a 1024x1024 pixels STEM image in the ETEM. The dose was controlled by changing the dwell time per pixel in the range 0.5–400 µs. The curves shown in Figure 3 are plotted as a function of area dose defined as $D=I_{0A}\tau_A/(\Delta x_A)^2$, where I_{0A} is the beam current, τ_A is the dwell time per dot and Δx_A=500/1024 nm=0.49 nm is the pixel size. The thickness of the exposed square was estimated with the log-ratio method using electron energy-loss spectroscopy (EELS)[20]. The pattern thickness is normalized to the thickness of a highly exposed area, which is estimated to be ~50 nm from collapsed features. The contrast curves are characterized by an onset dose D_O, below which no organic product remains after development, a saturation dose D_{sat}, after which the thickness of the pattern does not increase further, and a contrast, defined as $\gamma=1/\log_{10}(D^*/D_O)$. D_O and D^* are determined by extrapolating the linear portion of the contrast curve to 0 and 100%, respectively. The comparison between the measured contrast curves reveals a key finding: the onset dose decreases significantly with increasing molecular weight (Figure 3d), and follows an inverse proportionality trend observed for much heavier polymers[21]. The contrast also decreases with increasing molecular weight. It should be noted that the contrast of C_8H_{18} and $C_{11}H_{24}$ ice resists are 1.62 and 1.43, respectively, and that of $C_{14}H_{30}$ is only 0.18, indicating that these linear hydrocarbons are low sensitivity resists, which may be unsuitable for dense patterns. The correlation of D_{sat} with molecular weight is less obvious: it appears to decrease in undecane compared to octane, but then increases for tetradecane. The observed trends of onset dose, contrast and saturation dose for OIR are compared to polystyrene resists with different molecular weights[22] in the Supporting Information (Figure S7), confirming that the trend in D_{sat} is unusual.

In general, the linewidth and contrast curves obtained with negative EBL resists depend on many parameters such as resist material, exposure dose, beam size and energy, writing protocol and development process[23]. However, two general trends are observed[22–24]. First, high resolution resists require higher doses to achieve onset and saturation conditions. Second, with identical chemical structure and lithography protocol, resists

with a lower molecular weight are expected to deliver smaller features. The resolution limit for individual features was studied on chain-structure polystyrene as a function of molecular weight[21]. The dot diameter decreased from 25 to 10 nm with molecular weight decreasing from 17000 to 800 g/mol.

The conventional EBL process is based on the solubility variation of the irradiated region due to the change in molecular weight[23]. In contrast, OIRL is based on the change in critical solid-(liquid)-vapor phase transition temperature T_{cr}. Figures 4a,b illustrate schematically how an OIR contrast curve would be generated. The black lines in Figure 4a represent the molecular weight distribution in OIR before ($f_0(M)$) and after ($f_{D1}(M)$, $f_{D2}(M)$, $f_{D3}(M)$) e-beam exposure for doses *D1, D2, D3.* M_0 is the initial molecular weight of the organic precursor. The red curve in Figure 4a represents the expected dependency of T_{cr} on molecular weight, based on the melting points data for linear hydrocarbons[25]. M_{crit} marks the molecular weight above which the compound becomes non-volatile at temperature T_h. Exposing a hydrocarbon with initial molecular weight distribution $f_0(M)$ crosslinks the molecules and forms a new distribution $f_D(M)$. We expect the average molecular weight and the width of the distribution to increase with the dose. If the entire distribution $f_D(M)$ lies below a critical value M_{crit}, all molecules will leave the substrate after heating ($f_{D1}(M)$). This occurs at doses smaller than the onset dose D_O (Figure 4b), where the OIR contrast curve is zero. Above D_O and below D_{sat}, M_{crit} lies somewhere within the distribution ($f_{D2}(M)$), and only the fraction of the molecules with $M>M_{crit}$ remains after development, producing the portion of the contrast curve in the range $D_O<D<D_{sat}$. Above the saturation dose ($D>D_{sat}$) the entire distribution $f_D(M)$ lies above M_{crit}, and all molecules remain after sublimation. This description implies that organic precursors with larger initial molecular weight require less crosslinking events, and therefore lower doses, to cross the M_{crit} threshold and form a T_h-stable product. This behavior should manifest in lower onset and saturation doses (Figure 4c). For smaller molecules (M_0', Figure 4c), these doses are higher. Experimental contrast curves (Figure 3a-c) show that it is indeed the case for the onset doses.

However, two features of the experimental contrast curves cannot be explained solely by the simple mechanism described above: the trend of saturation doses, and the change in slope observed for octane at ~70 mC/cm^2 and for undecane at ~30 mC/cm^2 (marked with blue arrows in Figure 3a,b). These observations suggest that the change in T_{cr} from the exposure may not be uniquely defined by a change of molecular weight, and that some other factor may be in play that influences the shape of the contrast curves. Aside from molecular weight, the physical properties of organic compounds, including critical temperatures, depend on intermolecular forces, which in turn depend on molecular symmetry and architecture[26,27]. For example, linear n-octane has a melting point T_m=-57 ^{o}C. Its isomers 3-methylheptane and 2,5-dymethylhexane have lower melting points -122 ^{o}C and -93 ^{o}C, respectively. However, the octane isomer tetramethylbutane has a much higher melting point T_m=98 ^{o}C. This suggests that instead of a single threshold M_{crit}, we deal with a distribution of critical molecular weights applicable to various types of topologies of crosslinked structures. Consequently, the fraction of molecules remaining after heating depends both on the increase in average molecular weight and on the change in molecular shape. Achieving a deeper understanding of molecular shape evolution with dose and its effect on contrast curves requires separate investigations involving Molecular Dynamics and Monte Carlo simulations.

However, our experimental observations clearly indicate that feature size and onset doses correlate with the initial precursor molecular weight. In order to understand better these correlations, we need to determine how the onset dose relates to the patterned linewidth. The characteristics of patterned features in the form of isolated dots or lines depend on the beam profile, especially on the beam tails where the dose rate (beam current density) drops. With a Gaussian beam, the onset dose determines the feature size as illustrated in Figure 5a. Away from the Gaussian center, the degree of crosslinking is not sufficient for the exposed ice to become non-volatile at heating temperature T_h. Precursors with higher onset doses D_O will, therefore, result in smaller feature sizes.

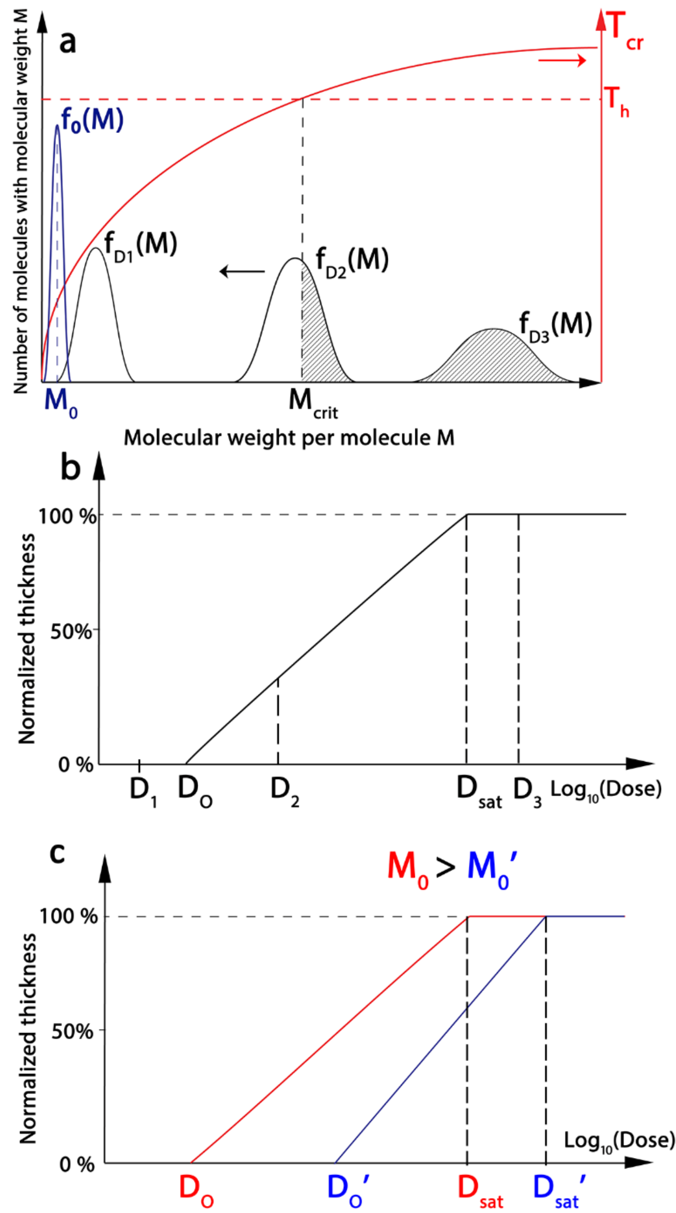

Figure 4. OIR contrast curve formation by e-beam exposure and thermal development. (a) Left Y axis: molecular weight distribution in OIR before ($f_0(M)$) and after ($f_{D1}(M)$, $f_{D2}(M)$, $f_{D3}(M)$) e-beam exposure for doses $D1$, $D2$, $D3$. M_0 is the initial molecular weight of organic precursor. Right Y axis: critical temperature dependency on molecular weight. Molecular weight M_{crit} defined as $T_{sub}(M_{crit})=T_h$. (b) Corresponding contrast curve: the normalized pattern thickness at a particular dose D depends on the shape of the molecular weight distribution $f_D(M)$, and on how its position with respect to M_{crit}. (c) Contrast curves for two precursors with different initial molecular weights M_0 and $M_0' < M_0$. Organic ices with lower molecular weight require more crosslinking events to produce a non-volatile product, therefore their contrast curves have higher values of onset ($D_O' > D_O$) and saturation doses ($D_{sat}' > D_{sat}$).

We consider a primary electron beam with a Gaussian profile, peak beam current density j_0 and beam radius R_p:

$$j_p(r) = j_0 e^{-\frac{r^2}{2R_p^2}}. \tag{1}$$

We expect crosslinking to occur mainly due to secondary electrons (SEs) for two reasons: i) we pattern a thin layer on a very thin substrate with 80 keV electrons, making the influence of backscattered electrons negligible; ii) any relevant inelastic cross section from 80 keV primaries is negligible with respect to that at the energy range (<50 eV) of SEs, since the cross section drops with $1/E$[28]. Even if the ~10000x drop in cross section may be partially offset if the effective yield of generated secondaries is below unity, the role of primaries in the exposure process may be safely neglected. Therefore, we assume that the electron flux driving the exposure process is

$$j_{SE}(r) = Y j_0 e^{-\frac{r^2}{2R_S^2}}, \tag{2}$$

where Y is an effective yield of generated SEs, representing the statistical number of SEs generated per primary, and R_s is the Gaussian radius of the spatial distribution of SEs, which we roughly expect to be $R_S \approx \sqrt{R_p^2 + \lambda^2}$, where λ is the inelastic mean free path of SEs at their mean energy. Therefore, the dose received by the ice over a time interval τ as a function of position $r = \sqrt{x^2 + y^2}$ is

$$D_{SE}(r) = Y j_0 \tau e^{-\frac{r^2}{2R_S^2}}. \tag{3}$$

When patterning a line (Figure 5b) or an area with overlapping beams we need to consider the contribution from the exposure of neighboring dots. In the assumption $\Delta x_L \leq R_s$ (significant overlap) the dot dose in a line D_L can be estimated as:

$$D_{SE_L}(y) = Yj_{0L}\tau_L\left[\dots + e^{-\frac{(-\Delta x)^2+y^2}{2R_S^2}} + e^{-\frac{y^2}{2R_S^2}} + e^{-\frac{(\Delta x)^2+y^2}{2R_S^2}} + \cdots\right] = Yj_{0L}\tau_L\, e^{-\frac{y^2}{2R_S^2}}\left[\sum_{i=-\infty}^{+\infty} e^{-\frac{(i\Delta x)^2}{2R_S^2}}\right] \approx \tag{4}$$

$$\approx Yj_{0L}\tau_L\left(\frac{\sqrt{2\pi}R_s}{\Delta x_L}\right)e^{-\frac{y^2}{2R_S^2}}$$

Following the same logic, dot dose in area is $D_{SE_A} = Yj_{0A}\tau_A\left(\frac{\sqrt{2\pi}R_S}{\Delta x_A}\right)^2$. j_{0L}, τ_L, j_{0A}, τ_A are primary beam current density, dwell time for line and area patterning, respectively. The patterned linewidth *d=2y_{DO}* (Figure 5b) can be found by solving the equation $D_{SE_L}(y_{DO}) = (D_{SE})_O = (D_{SE_A})_O$:

$$Yj_{0L}\tau_L\left(\frac{\sqrt{2\pi}R_S}{\Delta x_L}\right)e^{-\frac{y_{DO}^2}{2R_S^2}} = Y(j_{0A})_O(\tau_A)_O\left(\frac{\sqrt{2\pi}R_S}{\Delta x_{AO}}\right)^2. \tag{5}$$

Here $(j_{0A})_O$, $(\tau_A)_O$ and Δx_{AO} are area patterning parameters for the onset condition. As previously stated, the *experimental* onset dose D_O is defined as $D_O = \frac{I_{0A}(\tau_A)_O}{\Delta x_A{}^2} = \frac{j_{0A}(\tau_A)_O}{\Delta x_A{}^2}\pi R_p^2$. Therefore, the linewidth is expressed as:

$$d = 2y_{DO} = 2\sqrt{2}R_S\sqrt{\log\left(\frac{I_{0L}\tau_L}{\sqrt{2\pi}D_O R_S \Delta x_L}\right)}. \tag{6}$$

We have used equation (6) as a model function to fit the experimental linewidths as a function of beam current (Figure 5c) with D_O and R_s as fit parameters. All three data sets were fitted simultaneously with R_s as a common/shared parameter. Onset doses determined from the fit follow the same trend as experimental ones. The observed systematic mismatch can be attributed to the fact that we excluded the likely R_s dependence on material and, as discussed, contributions from primary beam and other sources[29].

The analysis of the experimental data and the model both suggest that a precursor with smaller molecular weight combined with a decrease in the line dose could produce sub-4 nm features. Indeed, by decreasing the beam current down to (0.21 pA) we patterned 3-nm lines on octane (see Supporting Information, Figure S5), which were, however, fragmented. This result indicates that the practical feature size limit is defined by stochastic effects[30]. By lowering the beam current we are decreasing the number of crosslinking events, but

in doing so we also enhance statistical fluctuations along the patterned line. These fluctuations result in line roughness and fragmentation and are the main factor controlling the ultimate feature size limit.

In conclusion, OIRL is a new approach to nanopatterning that works with small organic molecules, which are difficult to be accessed by other techniques. After e-beam irradiation, molecules within the exposed areas are crosslinked and their solid/vapor phase transition temperatures raises. Therefore, OIRL does not require chemical development and allows the removal of the unexposed molecules by heating. The technique has no limitation on what kind of substrates or functional substrates it can handle, and can be cycled in-situ to achieve direct 3D nanopatterning.

Aiming at achieving full control over the result of the exposure process in view of tuning its characteristics and properties, in this work we have taken a step towards understanding the physical and chemical processes occurring when OIRs are irradiated by an electron beam. To establish a link between resist characteristics and outcome of the OIRL process, we have patterned linear hydrocarbons of varying molecular weight. Our results show that OIR precursors with lower molecular weight produce smaller features under the same patterning conditions. We have successfully fabricated small continuous features down to 4.5 nm, and, more importantly, learned how to control the feature size by choosing a specific combination of beam and material parameters. With fixed beam parameters, the pattern size is primarily controlled by the onset dose, which we found to be inversely proportional to the precursor molecular weight. This trend, observed experimentally in polymer-based resists with much larger molecular weight, confirms that organic ices behave as regular negative tone resists, ensuring full compatibility of OIRL with existing lithographic protocols, while also opening new fields of application. Currently, we are focusing our efforts towards the use of OIRL in nanoscale additive manufacturing of functional materials, and biocompatible hydrogels for tissue engineering and soft robotics.

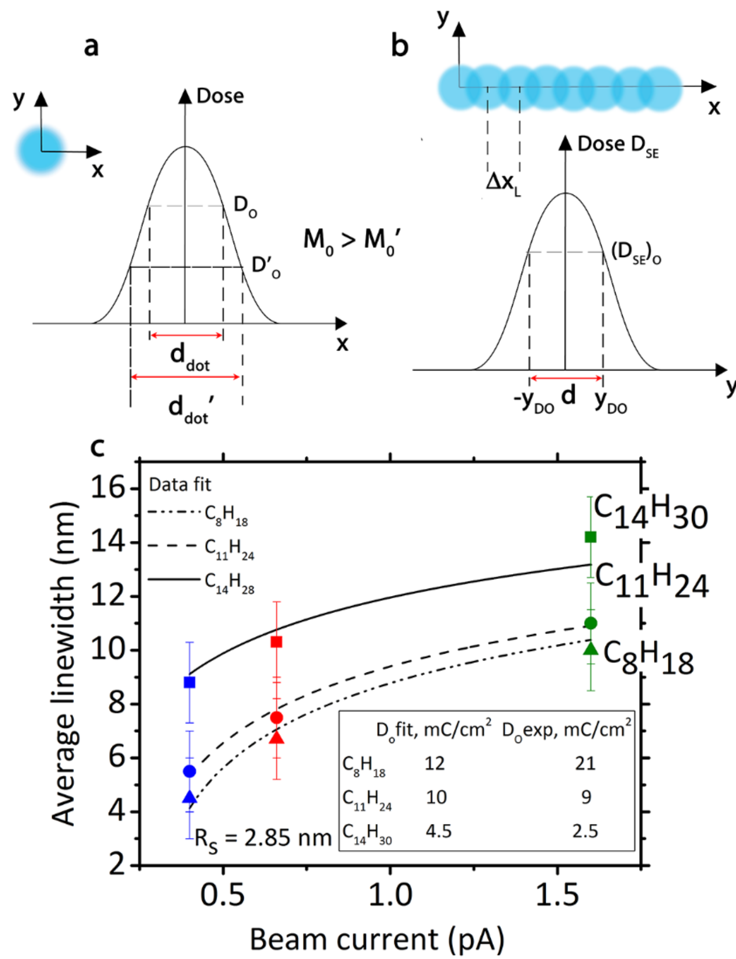

Figure 5. (a) Effect of Gaussian beam shape and the onset doses D_o and D_o' on the resulting isolated feature sizes d_{dot} and d_{dot}', respectively. (b) Effect of secondary electrons Gaussian beam shape and contribution from the exposure of neighboring pixels on the resulting line feature size. (c) Experimental values of linewidths as a function beam current I_{0L} fitted to Equation (6) with values of onset doses as parameters. Three datasets were fitted simultaneously with R_s as common parameter.

Author information

Corresponding author

Email: marco.beleggia@cen.dtu.dk

Author contributions

The experiments were designed by A.E., A.H. and M.B., and carried out by A.E.; modelling and data analysis were performed by A.E. and M.B.; A.E. drafted the manuscript; A.E. and D.Z. created the illustrations; all the authors discussed the results and contributed to writing and revisions of the manuscript.

Notes

The authors declare no competing financial interests.

Acknowledgments

A.E. and M.B. acknowledge financial support from the VILLUM foundation. D.Z. acknowledges funding from the EU Horizon 2020 Marie Skłodowska-Curie Actions, H.C. Ørsted COFUND, grant agreement No. 713683.

References

(1) Pi, S.; Ghadiri-Sadrabadi, M.; Bardin, J. C.; Xia, Q. *Nat. Commun.* **2015**, *6* (1), 7519.

(2) Ladd, T. D.; Jelezko, F.; Laflamme, R.; Nakamura, Y.; Monroe, C.; O'Brien, J. L. *Nature* **2010**, *464* (7285), 45–53.

(3) Jahani, S.; Jacob, Z. *Nat. Nanotechnol.* **2016**, *11* (1), 23–36.

(4) Geim, A. K.; Grigorieva, I. V. V *Nature* **2013**, *499* (7459), 419–425.

(5) Aspelmeyer, M.; Kippenberg, T. J.; Marquardt, F. *Rev. Mod. Phys.* **2014**, *86* (4), 1391–1452.

(6) Sparreboom, W.; van den Berg, A.; Eijkel, J. C. T. *Nat. Nanotechnol.* **2009**, *4* (11), 713–720.

(7) Faia-Torres, A. B.; Goren, T.; Textor, M.; Pla-Roca, M. C*omprehensive Biomaterials*; Elsevier, **2011**, 181–201.

(8) Christman, K. L.; Enriquez-Rios, V. D.; Maynard, H. D. *Soft Matter* **2006**, *2* (11), 928.

(9) Nie, Z.; Kumacheva, E. *Nat. Mater.* **2008**, *7* (4), 277–290.

(10) Bat, E.; Lee, J.; Lau, U. Y.; Maynard, H. D. *Nat. Commun.* **2015**, *6* (1), 6654.

(11) von Freymann, G.; Ledermann, A.; Thiel, M.; Staude, I.; Essig, S.; Busch, K.; Wegener, M. T *Adv. Funct. Mater.* **2010**, *20* (7), 1038–1052.

(12) Gangnaik, A. S.; Georgiev, Y. M.; Holmes, J. D. *Chem. Mater.* **2017**, *29* (5), 1898–1917.

(13) Hagen, C. W. *Appl. Phys. A* **2014**, *117* (4), 1599–1605.

(14) Han, A.; Vlassarev, D.; Wang, J.; Golovchenko, J. A.; Branton, D. *Nano Lett.* **2010**, *10* (12), 5056–5059.

(15) Tiddi, W.; Elsukova, A.; Le, H. T.; Liu, P.; Beleggia, M.; Han, A. *Nano Lett.* **2017**, *17* (12), 7886–7891.

(16) Tiddi, W.; Elsukova, A.; Beleggia, M.; Han, A. *Microelectron. Eng.* **2018**, *192*, 38–43.

(17) Hong, Y.; Zhao, D.; Liu, D.; Ma, B.; Yao, G.; Li, Q.; Han, A.; Qiu, M. *Nano Lett.* **2018**, 18(8), 5036-5041.

(18) Hu, X.; Wang, H.; Zhai, C.; Ge, H.; Cui, Y. *J. Mater. Chem. C* **2016**, 4(47), 11104-11109.

(19) Mølgaard Mortensen, P.; Willum Hansen, T.; Birkedal Wagner, J.; Degn Jensen, A. *Ultramicroscopy* **2015**, *152*, 1–9.

(20) Malis, T.; Cheng, S. C.; Egerton, R. F. *J. Electron Micr. Tech.* **1988**, *8* (2), 193–200.

(21) Manako, S.; Fujita, J.; Ochiai, Y.; Nomura, E.; Matsui, S. *Jpn. J. Appl. Phys.* **1997**, *36* (Part 2, No. 6A), L724–L726.

(22) Dey, R. K.; Cui, B. *Nanotechnology* **2013**, *24* (24), 245302.

(23) Grigorescu, A. E.; Hagen, C. W. *Nanotechnology* **2009**, *20* (29), 292001.

(24) Chen, Y. *Microelectron. Eng.* **2015**, *135*, 57–72.

(25) Mandelkern, L.; Prasad, A.; Alamo, R. G.; Stack, G. M. *Macromolecules* **1990**, *23* (15), 3696–3700.

(26) Reusch, W. H. *An Introduction to Organic Chemistry*; Holden-Day, **1977**.

(27) Jabbarzadeh, A.; Atkinson, J. D.; Tanner, R. I. *Macromolecules* **2003**, 36(13), 5020-5031

(28) Egerton, R. F. *Electron Energy-Loss Spectroscopy in the Electron Microscope*; Springer, **2011**.

(29) Manfrinato, V. R.; Wen, J.; Zhang, L.; Yang, Y.; Hobbs, R. G.; Baker, B.; Su, D.; Zakharov, D.; Zaluzec, N. J.; Miller, D. J.; Stach, E. A.; Berggren, K. K. *Nano Lett.* **2014,** 14(8) 4406-4412

(30) Ocola, L. E.; Stein, A. *J. Vac. Sci. Technol. B.* **2006**, *24* (6), 3061.

Supporting Information Available: description of the experimental procedures and guidelines for patterning organic ice resists in the TEM; patterning 3-nm lines on octane; width estimation of the patterned lines from bright-field TEM images; onset dose, contrast and saturation dose in OIRs and polystyrene resists with different molecular weights.